

DYNAMICS OF PRIMARY AND SECONDARY VORTICES IN A SLOT JET

Maxim V. Shestakov^{1,2}, Vladimir M. Dulin^{1,2}, Mikhail P. Tokarev^{1,2}, Dmitriy M. Markovich^{1,2*},

1: Kutateladze Institute of Thermophysics,

1, Lavrentyev Avenue, Novosibirsk, 630090, Russia

2: Department of Science and Research,
Novosibirsk State University

2, Pirogova Street, 630090, Russia

* dmark@itp.nsc.ru

FOCUS OF THE STUDY

The paper reports on results of 3D velocity measurements in a turbulent slot jet by tomographic particle image velocimetry (tomographic PIV; see review by Scarano, 2013). The flow is a shallow-water jet, bounded by two parallel walls. The distance (h) between the walls is not bigger than the transversal size of the nozzle (d), i.e., $h/d \leq 1$. The results show that the turbulent transport and mixing in these flows is a multi-scale problem associated with dynamics of primary large-scale quasi-two-dimensional vortices and secondary longitudinal vortex filaments.

INTRODUCTION

Interest in the study of shallow and slot jets is the result of a number of peculiarities that make them different from free jets and channel flows. The development of Kelvin-Helmholtz (K-H) instabilities and the formation of vortex structures in this case are accompanied by the strong influence of wall friction, which leads to the existence of a variety of fundamentally different regimes, from classical Hele-Shaw regimes up to developed turbulent flows manifesting some features of 2D turbulence. Meanwhile, recent measurements using planar velocimetry methods reveal that secondary wall-normal flows occur during the evolution of a vortex dipole in shallow fluid layers (see Akkermans et al., 2008; Albagnac et al., 2013). Such secondary vortices also arise in isolated concentrated vortices, such as tornados, and are important because they can rapidly disintegrate primary vortices.

For a jet flow between two parallel walls (separated by a distance h) issuing from a rectangular nozzle (with a spanwise size d) in the streamwise direction x , K-H instability causes the roll-up of vortices in each shear layer. Furthermore, as Holdeman and Foss (1975) emphasised, secondary longitudinal vortices can also be produced by the nozzle corners in the same manner as in free rectangular jets. Rockwell (1977) noted that core filaments of the K-H vortices rolling-up in the shear layers are curved downstream due to the velocity gradient near the walls. Thus, each stretched and inclined vortex tube causes the production of a streamwise vorticity component near each wall. Although these two models for the origin

of the secondary currents are different, the boundary layers enhance the production of the longitudinal vorticity.

Downstream of the nozzle exit, in contrast to rectangular free jets (Deo et al., 2007), the centreline velocity of shallow jets decays according to $x^{-1/2}$, and the width grows linearly with x , as in planar jets. Many studies report that the dynamics of shallow and slot jet flows are associated with jet meandering. This feature is associated with zigzag arrangement of the growing downstream K-H vortices with an opposite direction of rotation for each subsequent vortex. A stability analysis by Daoyi and Jirka (1998) shows that for high Reynolds numbers, this sinuous flow instability dominates for linearly expanding jets for the bed-friction parameter $S = c_f b_{1/2}/h$ (c_f is the wall friction coefficient; $b_{1/2}$ is the jet half width) below a critical value of approximately 0.7 (without a co-flow).

Meanwhile, the dynamics of shallow and slot jets (far from the nozzle exit) are usually considered as the propagation of large-scale quasi-2D structures (with a size considerably larger than h) over smaller-scale 3D turbulence (with scales of less than h). The measured spectra of the shear stress and velocity fluctuations clearly exhibit a slope of -3 for the long-wave domain (Dracos et al., 1992; Chinak et al., 1995; Rowland et al., 2009). This attribute of 2D turbulence becomes more pronounced for smaller h/d . However, the results of the proper orthogonal decomposition (POD, see Holmes et al., 1996) of the velocity fields, measured by PIV by Shinneeb et al. (2011), indicate that jet flow meandering and the dynamics of quasi-2D structures are also accompanied by coherent velocity fluctuations in the wall-normal direction. Thus, 3D large-scale flow organisation in shallow and slot jets is still not completely understood.

The objective of the present work is to investigate dynamics of large-scale vortex structures in slot jets ($h \leq d$) by using modern 3D velocimetry method.

EXPERIMENTAL SETUP AND DATA PROCESSING

The slot jet flow was organized in a closed hydrodynamic circuit, included a tank, pump, flow meter, and test section. The test section represented a plane channel formed by two plates of organic glass (with longitudinal and transverse dimensions of 307 and 270

mm, respectively, and 20 mm in thickness), separated by a distance $h = 4$ mm. The non-contracting nozzle is a rectangular channel ($h \times d$ cross-section) with $20h$ in length, connected to a honeycomb. The transversal size d of the nozzle was set to 4 or 10 mm.

A schematic of the studied slot jets is shown in Figure 1. The jet flow is described using a Cartesian coordinate system. The components of $\mathbf{x} = (x, y, z)$ correspond to the spanwise, streamwise, and wall-normal directions, respectively. The origin of the coordinate system is defined as the centre of the rectangular nozzle exit. The mean velocity vector is denoted by $\mathbf{U} = (V, U, W)$.

The experiments were carried out for two Reynolds numbers: 10^4 and 2×10^4 . The Reynolds number is denoted as $Re = 2HU_b/\nu$, where U_b is the bulk flow velocity, H is the hydraulic diameter for the rectangular nozzle, and ν is the water kinematic viscosity.

To provide PIV measurements, the flow was seeded with $50 \mu\text{m}$ polyamide particles. The measurement system consisted of a high-repetition pulsed Nd:YAG laser (Photonix DM-532-100), four high-speed CMOS cameras (Photron FASTCAM SA5), and synchronizing device Berkeley Nucleonics BNC 575. The laser beam was converted to a thick laser sheet, which illuminated the entire channel between the glass plates (see Figure 2). The cameras were equipped with SIGMA AF 105 mm $f/2.8$ EX DG MACRO lenses.

The size of the measurement volume was $64 \times 64 \times 4$ mm³. For each flow case, the measurements were performed for three overlapping fields of view (FOV). For each FOV, twenty one thousand of 1024×1024 images were captured by each camera with acquisition rate of 10 kHz. Besides, the frequency was 25 kHz for some flow regions with a smaller FOV.

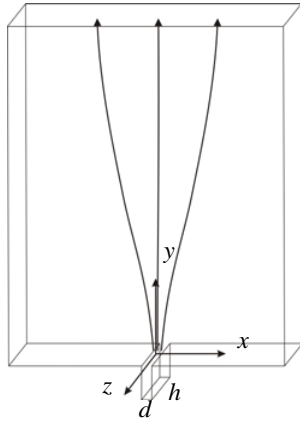


Figure 1. Schematic of the slot jet flow and coordinates system

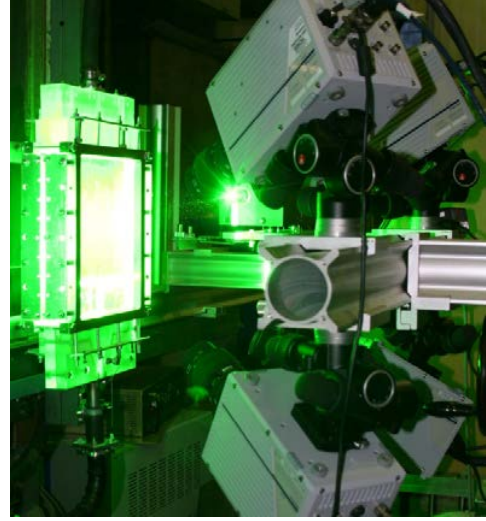


Figure 2. Photo of the experimental setup

A plane target (Edmund Optics 50×50 mm²) was fixed inside the slot to calibrate of the camera system. A precise traverse system shifted the cameras relative to the calibration target. The cameras were equipped with 3D printed Scheimpflug adapters to align the focal plane to the sensor plane.

In-house “ActualFlow” software was used to measure and process the acquired images. A self-calibration procedure (similar to that of Wieneke, 2008) was applied prior to the tomographic reconstruction of 3D images. It was performed in three steps. The final average disparity was below 0.05 pixels, and the maximum corrected disparity was equal to 4 pixels. Also, before the reconstruction step, the recorded projections were pre-processed by subtracting the statistical minimum of intensity for each pixel.

The size of the reconstructed 3D images was $1024 \times 1024 \times 128$ voxels. The tomographic reconstruction was done by a MLOS-SMART method (Atkinson and Soria et al., 2009). Particles shift was evaluated by using an iterative multi-grid algorithm with continuous interrogation box shifting. The spatial grid-overlap factor was set to 50%. The correlation domain size for calculation of each velocity vector was $1 \times 2 \times 0.5$ mm³ ($16 \times 32 \times 16$ voxels).

RESULTS

The centreline velocity is shown in Figure 3. The data are shown for $Re = 2 \times 10^4$ and 10^4 and for $d/h = 2.5$ and 5. When normalised by d , the velocity profiles collapse, and the centreline velocity profile corresponds to $(x - x_0)^{-1/2}$, as in planar jets.

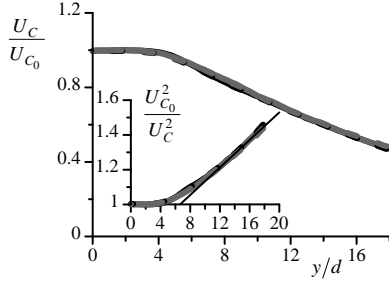


Figure 3. Centreline velocity in slot jets. The grey and black lines (almost completely coincide) correspond to $d/h = 2.5$ and 5 and for $Re = 2 \times 10^4$ and 10^4 . The inset shows the centreline velocity to the power of -2 and a linear fit function (thin line)

Further we discuss on 3D flow organisation near the nozzle exit. Only the case with $Re = 2 \times 10^4$ is considered. Figure 4 shows the velocity distributions in the middle plane (that passes through the jet axis and is parallel to the walls) of the time-averaged 3D velocity field. The field of view covers the domain of $9h$ downstream of the nozzle exit and nearly $10h$ in the spanwise direction. The plot also contains surfaces corresponding to constant values of the streamwise component of the time-averaged velocity ($1.05U_0$) and vorticity ($\pm 0.15U_0/d$).

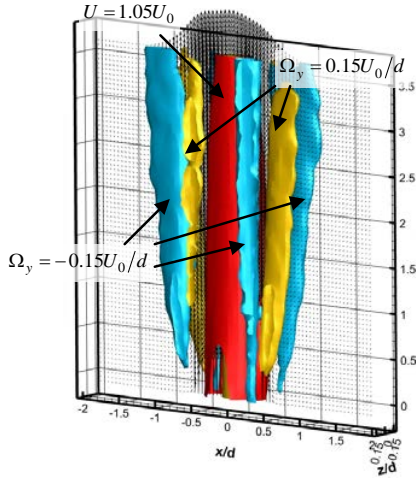


Figure 4. Time-averaged 3D velocity data for a slot jet at $d/h = 2.5$ and $Re = 2 \times 10^4$. Surfaces show constant values of the time-averaged streamwise velocity and vorticity.

As observed in both cases, eight regions of intensive longitudinal vorticity surround the jet core. Thus, each shear layer contains four domains with non-zero time-averaged vorticity. Similar time-averaged pattern is observed for the flow with $d/h = 1.0$ (see Figure 5). The pairs of domains with opposite vorticity in the outer region of each mixing layer are believed to be associated

with a stronger time-averaged entrainment in the middle plane, whereas the jet spreads faster at $z/h = \pm 0.45$ (see Bilsky et al., 2013; Shestakov et al. 2014). Less intensive streamwise vortices closer to the jet core are considered to originate from corner flows inside the rectangular nozzle.

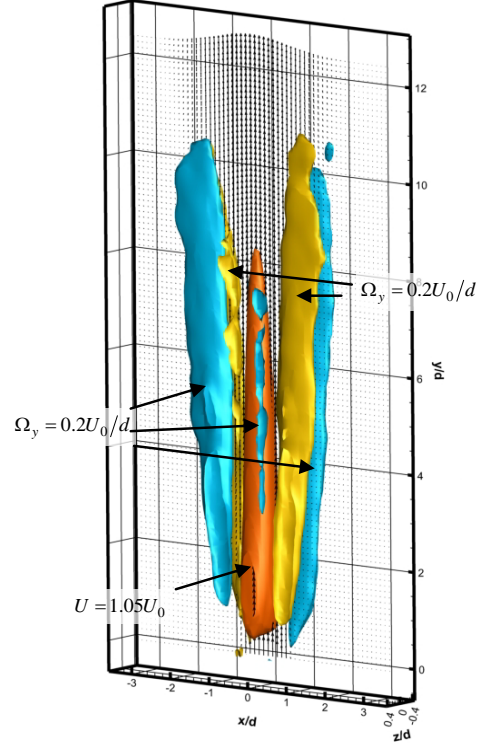


Figure 5. Time-averaged 3D velocity data for a slot jet at $d/h = 1$ and $Re = 2 \times 10^4$. Surfaces show constant values of the time-averaged streamwise velocity and vorticity.

Such structures were also observed earlier during single-point velocity measurements. As reported by Giger et al. (1991) and Dracos et al. (1992), based on the mean centreline velocity and on the intensity of fluctuations, the effects of the secondary currents are maximal at approximately $6d$, and they appear to vanish after $10d$ (Holdeman and Foss, 1975). However, as noted by Dracos et al. (1992), influence of longitudinal vortex structures on turbulence, intermittency and mixing in the initial region of the jet requires further studies.

POD was performed for the sets of three-dimensional velocity fields to identify the large-scale coherent structures and investigate their shape. For any spatial domain with \mathbf{x} , the POD approach is based on the representation of each i -th instantaneous velocity field \mathbf{u}_i^* as a finite series of products of spatial orthonormal basis functions $\boldsymbol{\varphi}_n$ with "time-dependent" coefficients a_n^i :

$$\mathbf{u}_i^*(\mathbf{x}) = \sum_{n=0}^N a_n^i \boldsymbol{\varphi}_n(\mathbf{x}), \text{ where } \langle \boldsymbol{\varphi}_i, \boldsymbol{\varphi}_j \rangle_{\Omega} = \delta_{ij} \quad (1)$$

Here, $\langle \cdot \rangle_{\Omega}$ denotes spatial averaging, and δ_{ij} is the Kronecker delta. Following the snapshot method by Sirovich (1987), the basis functions $\boldsymbol{\varphi}_n$ can be represented as the following sum:

$$\boldsymbol{\varphi}_n^*(\mathbf{x}) = \sum_{k=0}^N A_k^n \mathbf{u}_k^*(\mathbf{x}) \quad (2)$$

A variational problem for the optimal orthonormal basis (1) can be solved as a solution of a Fredholm integral equation of the second type, where the kernel of the integral operator is a cross-correlation function between the instantaneous velocity fields:

$$\frac{1}{N} \sum_{m=1}^N \langle \mathbf{u}_n(\mathbf{x}) \mathbf{u}_m(\mathbf{x}) \rangle_{\Omega} A_m^i = \lambda_i A_n^i \quad (3)$$

The solution to the eigenvector/eigenvalue problem (3) allows for the determination of N eigenvectors $\mathbf{A}^i = \{A_1^i \dots A_N^i\}$ and corresponding eigenvalues λ_i for calculating the POD basis functions $\boldsymbol{\varphi}_n$. By virtue of the matrix symmetry, the eigenvalues have the following property: $\lambda_i > 0$ (for any i). Additionally, it is possible to apply the following condition: $\lambda_{i-1} \geq \lambda_i \geq 0$ ($i = 1, \dots, N$).

In the present work, problem (3) was solved, considering the matrix symmetry, using a QR algorithm to reduce the correlation matrix. The zero POD mode $\boldsymbol{\varphi}_0$ corresponded to the mean velocity field \mathbf{U} , and λ_i was related to spatially averaged values of the squared velocity fluctuations for the given mode.

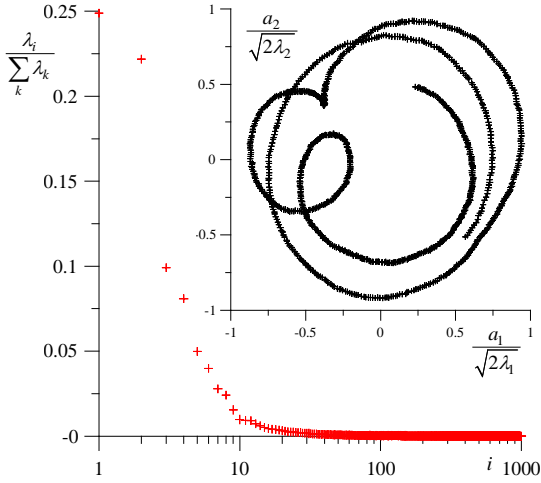


Figure 6. POD spectra of 3D velocity fields in a slot jet at $d/h = 2.5$ and $\text{Re} = 2 \times 10^4$. The inset shows correlation coefficients of the first and second POD modes

The spectrum of the decomposition for the slot jet at $d/h = 2.5$ and $\text{Re} = 2 \times 10^4$ is shown in Figure 6. The considered field of view covers streamwise direction from $7d$ to $12d$. Two the most powerful modes can be separated

from the other modes. These modes are associated with almost 50% of the spatially averaged turbulent kinetic energy in FOV of the flow. Besides, as the inset in Figure 6 demonstrates, the correlation coefficients of these two modes in the Lissajous plot produce a figure around a circle.

Figure 7 shows the velocity fluctuations (in the middle plane) associated with these two POD modes. The spanwise velocity component is visualised by colour. These two POD modes are associated with strong and long-wave flow oscillations with wavelength much greater than h (about $4d$). Thus, the modes represent longitudinal wave of velocity oscillations in the spanwise direction, and the POD distributions differ by shift with a quarter of the wavelength.

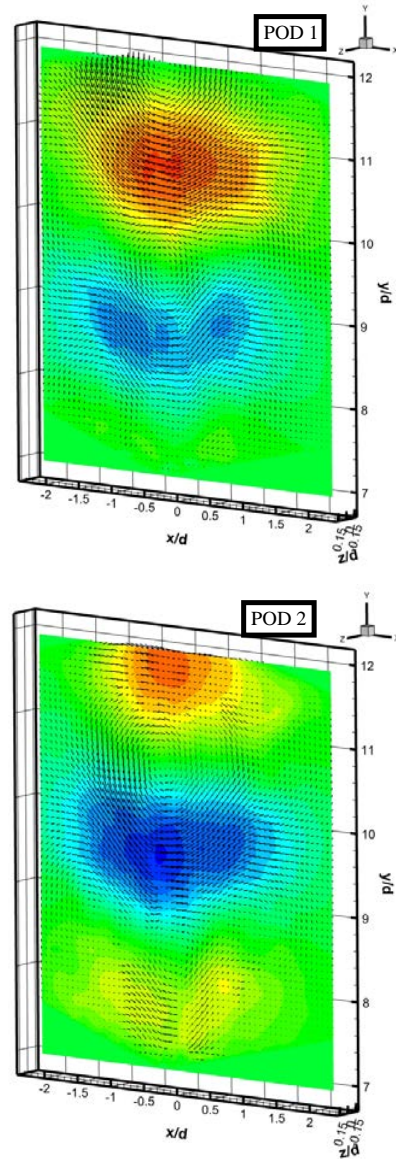


Figure 7. Visualisation of the most energetic POD modes in a slot jet at $d/h = 2.5$ and $\text{Re} = 2 \times 10^4$.

The bed friction parameter (Daoyi and Jirka, 1998) of the studied jet flows was much below of 0.7. This ensured sinuous jet instability: after a few d downstream the nozzle exit, the jet meandering took place and was accompanied by growth of large-scale quasi-two-dimensional vortices (with size much greater than h). They arranged in a zig-zag pattern, and the sense of rotation of each subsequent vortex was opposite to the previous one.

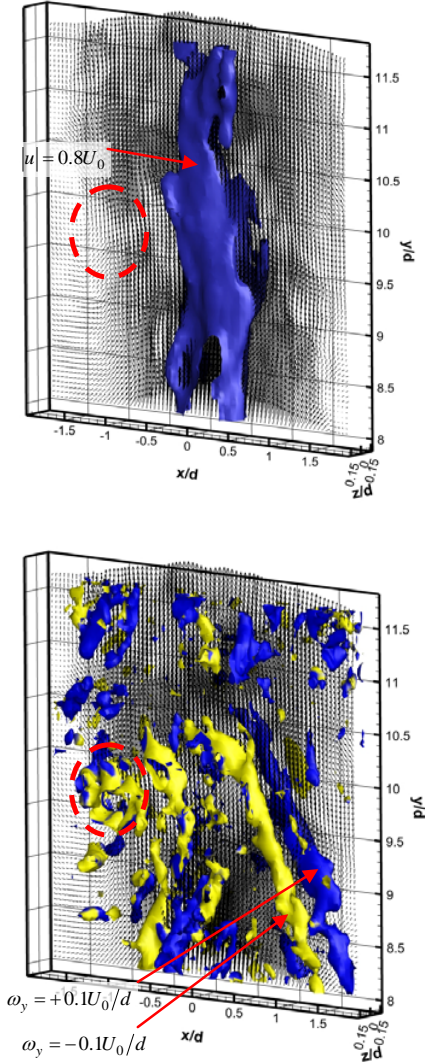


Figure 8. Visualisation of jet core (upper plot) and large-scale vortex structures ($Q = \text{const} > 0$ in the bottom plot) in the instantaneous velocity field in a slot jet at $d/h = 2.5$ and $Re = 2 \times 10^4$.

It is concluded that the most powerful POD modes are associated with the jet meandering. Note that Lissajous plot in figure 6 has loops, which are associated with decrease of the coherent mode amplitude. Thus, the

meandering amplitude was suppressed for some time instants, as it was predicted previously by Shestakov et al. (2014) from 2D PIV measurements.

Figure 8 shows the 3D flow organisation for a single 3D velocity snapshot in the slot jet for $d/h = 2.5$ and $Re = 2 \times 10^4$. The iso-surface $|u| = 0.8U_0$ is shown to demonstrate meandering of the jet core. The ellipse in the upper and bottom plots shows the location of a centre of quasi-two-dimensional large-scale vortex, determined from Q-criterion (Hunt et al., 1988). The iso-surfaces of positive Q criterion are coloured by local values of the streamwise vorticity. Two arrows in the bottom plot of Figure 8 point at two counter-rotating secondary longitudinal vortex structures, moving on the opposite side of the jet core.

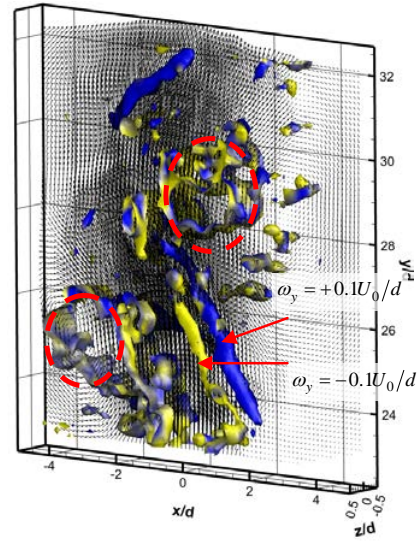


Figure 9. Visualisation of large-scale vortex structures ($Q = \text{const} > 0$) in the instantaneous velocity field in a slot jet at $d/h = 1.0$ and $Re = 2 \times 10^4$.

Figure 9 visualizes vortices in the jet with $d/h = 1.0$. The surfaces of Q criterion are also coloured by local values of the streamwise vorticity. This snapshot contains two opposite quasi-two-dimensional vortices marked by the ellipses. The jet meandering between the opposite vortices can be seen. At the same time, the secondary longitudinal vortex filaments are amplified, when the jet flow passes between two counter-rotating vortices.

CONCLUSIONS

The high-speed volumetric PIV measurements for the slot jet were performed to study new flow features. One of them is the modulation of the jet core meandering. Another one is the formation of the secondary longitudinal vortices in the far field of the jet. Such well-organized secondary vortices are known to be present in the mixing later of shallow jets near the nozzle exit. But, to our knowledge, such structures were not observed in far fields before.

ACKNOWLEDGEMENTS

This work is funded by Russian Science Foundation under grant No. 14-19-01685 (supervised by Prof. Markovich in the Institute of Thermophysics. The appreciate Dr. Mullyadzhanov and Prof. Hanjalic for useful discussions.

REFERENCES

- Atkinson, C.H. and Soria, J. 2009. An efficient simultaneous reconstruction technique for tomographic particle image velocimetry. *Experiments in Fluids*, Vol. 47, pp. 553–568.
- Akkermans, R.A.D., Cieslik, A.R., Kamp, L.P.J., Triefling, R.R., Clercx, H.J.H., and van Heijst, G.J.F. 2008. The three-dimensional structure of an electromagnetically generated dipolar vortex in a shallow fluid layer. *Physics of Fluids*, Vol. 20, 116601.
- Albagnac, J., Moulin, F.Y., Eiff, O., Lacaze, L., and Brancher, P. 2014. A three-dimensional experimental investigation of the structure of the spanwise vortex generated by a shallow vortex dipole. *Environmental Fluid Mechanics*, Vol. 14, pp. 957-970.
- Bilsky, A.V., Lozhkin, V.A., Markovich, D.M., and Tokarev, M.P. 2013. A maximum entropy reconstruction technique for tomographic particle image velocimetry. *Measurement Science and Technology*, Vol. 24, 045301.
- Chinak, A.V., Kashinsky, O.N., and Narkoryakov, V.E. 1995. Power spectra of shear stress fluctuations in turbulent flows. *Proceedings, Turbulence, Heat Mass Transfer 1*, K. Hanjalic and J.F.C. Pereira, eds., Begell House, pp. 71-75.
- Daoyi, C., and Jirka, G.H. 1998. Linear stability analysis of turbulent mixing layers and jets in shallow water layers. *Journal of Hydraulic Research*, Vol. 36, pp. 815-830.
- Deo, R.C., Nathan, G.J., and Mi, J. 2007. Comparison of turbulent jets issuing from rectangular nozzles with and without sidewalls. *Experimental Thermal and Fluid Science*, Vol. 32, pp. 596–606.
- Dracos, T., Giger, M., and Jirka, G.H. 1992. Plane turbulent jets in a bounded fluid layer. *Journal of Fluid Mechanics*, Vol. 241, pp. 587–614.
- Giger, M., Dracos, T., and Jirka, G.H. 1991. Entrainment and mixing in plane turbulent jets in shallow water. *Journal of Hydraulic Research*, Vol. 29, pp. 615-642.
- Holdeman, J.D., and Foss, J.F. 1975. The initiation, development, and decay of secondary flow in a bounded jet. *Journal of Fluids Engineering*, Vol. 97, pp. 342-352.
- Holmes, P., Lumley, J.L., and Berkooz, G. 1996. *Turbulence, coherent structures, dynamical systems and symmetry*. Cambridge University Press, Cambridge, UK.
- Hunt, J.C.R., Wray A.A., and Moin, P. 1988. Eddies, stream, and convergence zones in turbulent flows. *Center for Turbulence Research Report*, CTR-S88, p. 193
- Rockwell, D.O. 1977. Vortex stretching due to shear layer instability. *Journal of Fluids Engineering*, Vol. 99, pp. 240-243.
- Rowland, J.C., Stacey, M.T., and Dietrich, W.E. 2009. Turbulent characteristics of a shallow wall-bounded plane jet: experimental implications for river mouth hydrodynamics. *Journal of Fluid Mechanics*, Vol. 627, pp. 423–449
- Scarano, F. 2013. Tomographic PIV: principles and practice. *Measurement Science and Technology*, Vol. 24, 012001
- Shestakov, M.V., Dulin, V.M., Tokarev, M.P., Sikovsky, D.P., and Markovich, D.M., 2014. PIV study of large-scale flow organisation in slot jets. *International Journal of Heat and Fluid Flow*, Vol. 51, pp. 335-352.
- Shinneeb, A.-M., Bugg, J.D., and Balachandar, R. 2011. Coherent structures in shallow water jets. *Journal of Fluids Engineering*, Vol. 133, 011203.
- Sirovich, L. 1987. Turbulence and the dynamics of coherent structures Part I: Coherent structures *Quarterly of Applied Mathematics*, XLV, pp. 561-571
- Wieneke, B., 2008. Volume self-calibration for 3D particle image velocimetry. *Experiments in Fluids*, Vol. 45, pp. 549-456.